Crawler Design Document
ME 112

The Oh(l)ms

Jack Lane, Sonali Singh, Mario Khosla, Reed Kraus

Mechanical Engineering Design Group
416 Escondido Mall
Stanford University
Stanford, CA 94305-2203

1 Executive Summary

The challenge at hand was to design a machine capable of driving roughly 2 meters through a small (13.5 cm wide and 9 cm tall), gutter-like tunnel, littered with gravel and 1.75 cm steps. Upon reaching the end of the tunnel, the machine needed to capture a salamander, and bring it back to the start of the tunnel, with the ultimate goal of using as little energy as possible.

To design such a crawling machine, we began with a bill of materials solely consisting of Lego™ parts, adding ¼”-thick Duron, standard rubber bands, 18 gauge galvanized steel wire, and a few drops of olive oil as needed. Additionally, we were outfitted with a 5V-rated, brushed DC motor connected to a variable power supply. Our iterative process involved experimenting with different transmissions, catching mechanisms, wheels shapes, and bodies for our crawler. Figure 1, below, illuminates the final design of our crawler, weighing approximately 206 grams, utilizing front and rear wheel drive, with a transmission reduction of 75:1. During testing, it traveled at an average speed of 0.201 meters per second and consumed between 0.12 and 0.15 Amps of current at 3 Volts. Our crawler consumed 3.95 Joules of energy to complete the salamander retrieval task in testing, with an overall efficiency of 14.6%.

Our design was successful in consuming far less energy than the anticipated 40 Joules. Additionally, the salamander-catching mechanism has proven to be 100% effective in trial and testing. There is room, however, to improve the efficiency of our crawler, primarily by reducing weight, shifting the center of gravity of the crawler, changing our wheel design to reduce energy dissipation in collisions, and utilizing to a more efficient motor.

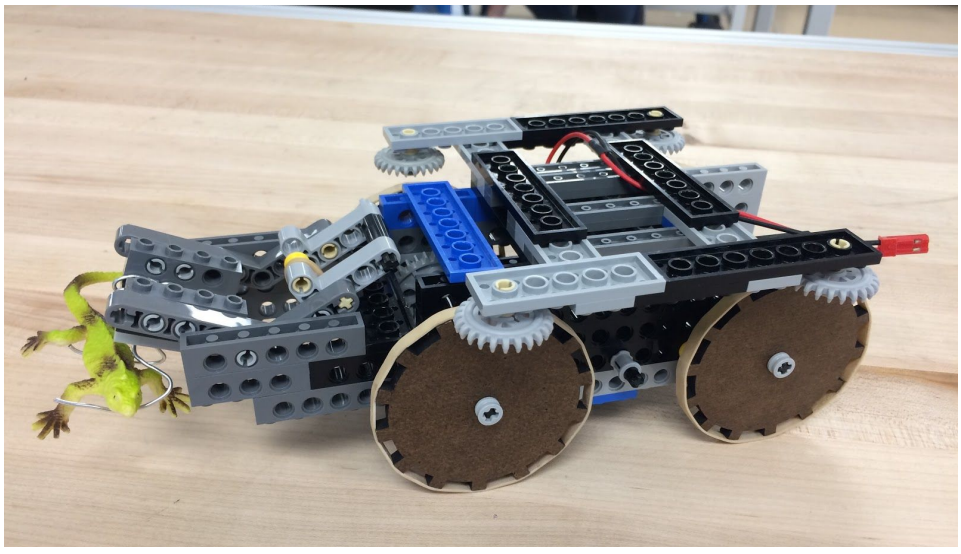

Fig. 1: *Our final salamander-catching machine holding a salamander in its mechanism*

Contents

1 Executive Summary **2**

2 Background **4**

3 Design **5**

3.1 Salamander Catching Mechanism 5

3.2 Transmission 7

3.3 Crawler Body 8

3.4 Linear Guides 9

3.5 Wheel Design 10

4 Logistics **12**

5 Performance Analysis **13**

5.1 Motor Performance 13

5.2 Transmission Performance 16

5.3 Rolling Resistance & Slippage 17

5.4 Efficiency Analysis 17

5.5 Gear Strength 18

6 Conclusion and ReDesign **20**

7 Appendices **21**

A1 - Symbols and Definitions 21

A2 - Motor Equations and Derivations 22

A3 - Motor Graphs and Data 23

A4 - Tests and Equations for Tests (Rolling, Transmission Efficiency) 26

A5 - Strength Calculations 26

A6 - Previous Prototypes 27

2 Background

In preparation for the California Tiger Salamander breeding season in the spring, it is imperative that the “Tunnel of Love” under Junipero Serra Boulevard is nicely covered in salamander pheromones, to coax the creatures into using the tunnel. This tunnel provides a safe path for the salamanders to cross from the lush Stanford hills to their breeding ground in Lake Lagunita, without getting run over by the busy traffic of Junipero Serra. Unfortunately, it is not trivial to teach a salamander to crawl through an artificial, concrete tunnel. As such, we needed to come up with a way of forcibly dragging a salamander through the tunnel, leaving a trail of pheromones in its wake. The machine designed to do this is intended to operate at 3V, 6V, or 8V, and must use 40 Joules or less of energy. The machine is intended run and catch the salamander autonomously, with the exception of us having to switch the leads of the motor-to-power connection. The catching of the salamander should also not do any permanent harm to the amphibian.

3 Design

The guiding principles of our crawler design were simplicity, repeatability, and reliability. To that end, the design for our crawler comprises four main components – the crawler body, the transmission, the salamander retrieval mechanism, and the linear guides. These components work in unison to allow for quick, efficient, and exceptionally reliable retrieval of the salamander. Below, the four main components are explored in more detail.

3.1 Salamander Catching Mechanism

The design of our crawler centered around the effectiveness of our salamander retrieval mechanism. The final design, a rubber-band-loaded fork with 18-gauge galvanized steel wire prongs on one end, is both elegant and reliable. The mechanism is mechanically triggered, requiring no control features to pick up or transport the salamander, and consistent, with a 100% success rate for salamander retrieval.

The mechanism design centers around the fact that a rubber band in tension will pull a lever arm in either a clockwise or a counter-clockwise direction, depending upon which side of the axel the rubber band rests (Fig. 3.1.1). In the loaded, or unfired, state, the rubber band rests below the axle and exerts a counter-clockwise moment on the lever arm. We calibrated the mechanism such that the rubber-band retains sufficient tension to hold the lever-arm in the loaded position as the crawler advances over the rough, gravel terrain of the track. As the crawler approaches the salamander, the end of the lever-arm makes contact with the wall. The force exerted by the wall activates pushes the lever arm up until the line-of-action of the rubber band is above the axle. At this point, the rubber band applies a clockwise moment to the lever-arm, firing the mechanism and swinging the wire prongs underneath the body of the salamander (Fig 3.1.2).

As the crawler retreats, the tension of the rubber band holds the mechanism in the fired state so that the salamander is safely suspended above the gravel. The catching fork is three-pronged, creating multiple points of contact and providing longitudinal support along the salamander body, ensuring that the amphibian does not escape during the return journey.

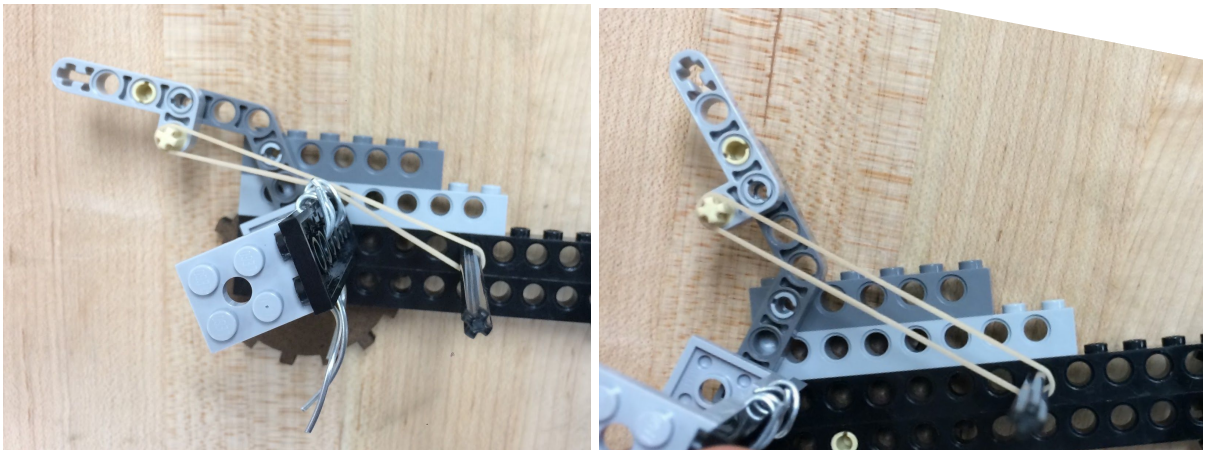

Figure 3.1.1 Internal view of a rubber-band-loaded mechanism prototype. Left: Rubber band below the lever axle in the unfired position. Right: Rubber band above the lever axle in the fired position.

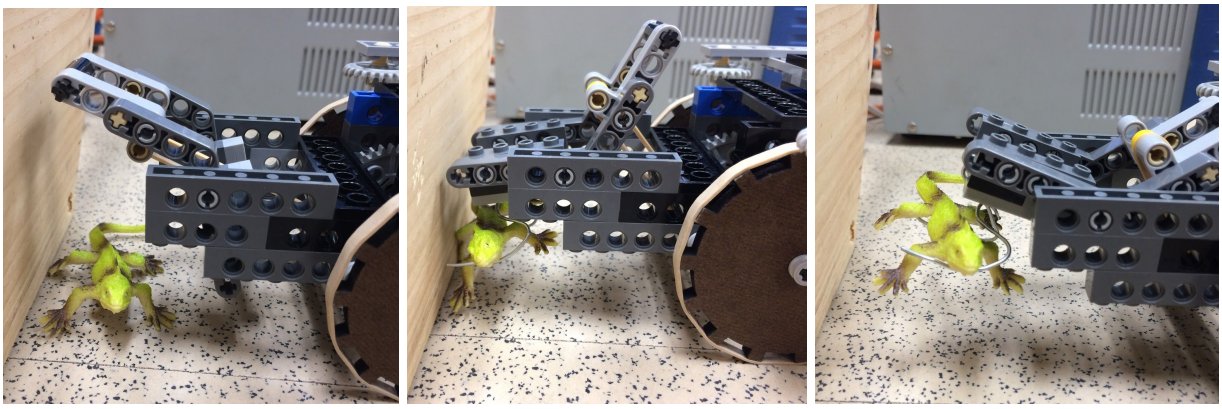

Figure 3.1.2: Left: Unfired mechanism as crawler approaches the wall and the salamander. Center: Fired mechanism after contact between end of lever arm and the wall Right: Salamander held in wire prongs

3.2 Transmission

Our transmission that utilized a pair of three stage reductions, for an overall reduction of 75:1 applied to both the front and rear wheels (Figure 3.2.1) . Figure 3.2.2 illustrates the center of gravity of our crawler, which is located approximately 2.5 cm behind the front axle and 7 cm away from the rear axle. This front-loaded center of gravity would render a rear-wheel-drive crawler useless on the return journey, as the rear wheels without sufficient downward force would not be able to gain enough traction in the gravel to drive the front wheels. As such, we chose to drive both the front and rear axles, avoiding the complications involved in repositioning the center of gravity for a rear-wheel-only transmission. Additionally, the gear ratio of 75:1 imparted sufficient torque, approximately 25 mNm (see Figure 5.1.3), to the front and rear axles, allowing both sets of wheels enough traction in the gravel and enabling the crawler to surmount steps in both forward and reverse.

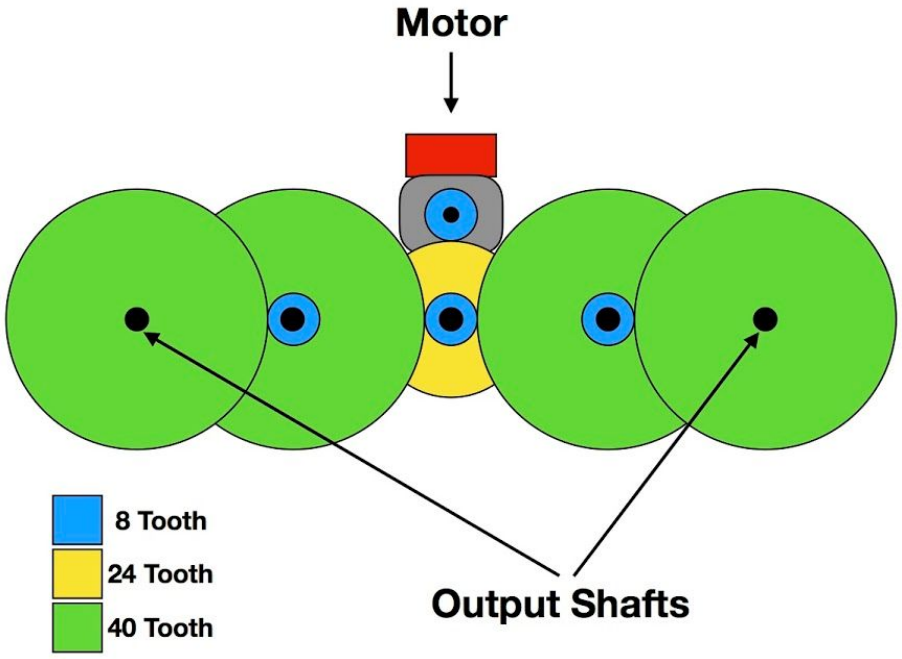

Figure 3.2.1 Internal schematic of our gear transmission.

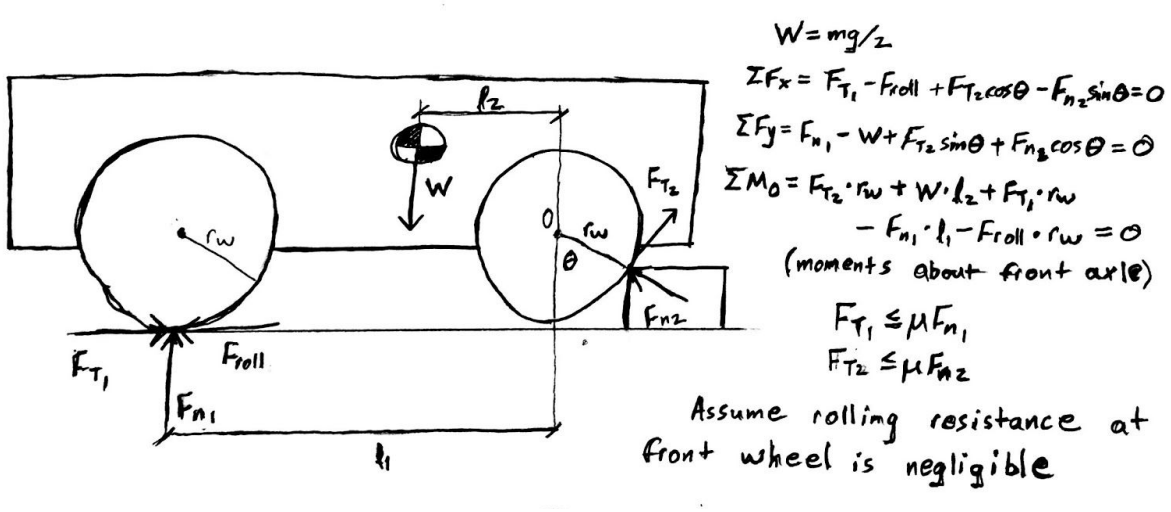

Figure 3.2.2: Free Body Diagram of the crawler immediately after the front wheels contact a step and leave the ground. The center of gravity of our crawler was approximately 2.5 cm (l_2) from the front axle of the vehicle.

3.3 Crawler Body

The body of our crawler served mainly as a mount for the rest of the components. In addition to being the foundation point for the linear guides and retrieval mechanism, it constrained and supported the transmission and held the drive axles stable. The transmission interconnectedness was the main driver of the size of the crawler body in that it was made to be as narrow, as short, and as low in height as possible while still fully enclosing, supporting, and protecting the gear linkages.

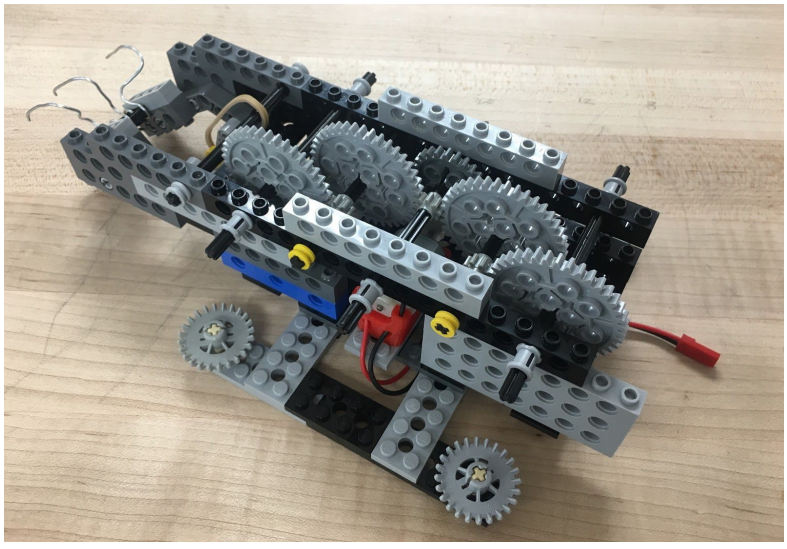

Figure 3.3.1: view of crawler body from bottom (without wheels)

The crawler body structure is depicted in Figure 3.3.1 below. It was cross-braced to add structural rigidity, mainly to decrease the twisting of the body as it travels. Smoothness of our transmission depended heavily the side walls of the crawler body being parallel. After constructing the transmission, the whole body was inverted, as shown in Figure 3.3.1. We did this to minimize the overall height of our crawler, given the position of the motor.

3.4 Linear Guides

In order to both increase the efficiency of our crawler and ensure the accuracy of our salamander retrieval mechanism, we outfitted our crawler with linear guides, depicted in Figure 3.4.1. These guides consist of freely rotating gears connected to the crawler body via lego scaffolding. The guides kept the crawler moving in a relatively straight line and prevented the sides of the crawler from rubbing or scraping along the inside of the track. We found that non-centered guides created a bias in our salamander locomotion toward one the side of the track, and therefore chose to center our guides over the body of the crawler. Centered guides also ensured that our salamander retrieval mechanism was properly aligned with the salamander on each run.

The guides are slightly more narrow than the full width of the track, allowing our crawler to roll freely with no added resistance in the ideal case that the crawler moves in a straight line. We never saw this ideal case during testing, however, because the interference between the gravel and the wheels always jolted the crawler to the left and right. Ultimately, the linear guides proved critical to the success of our crawler.

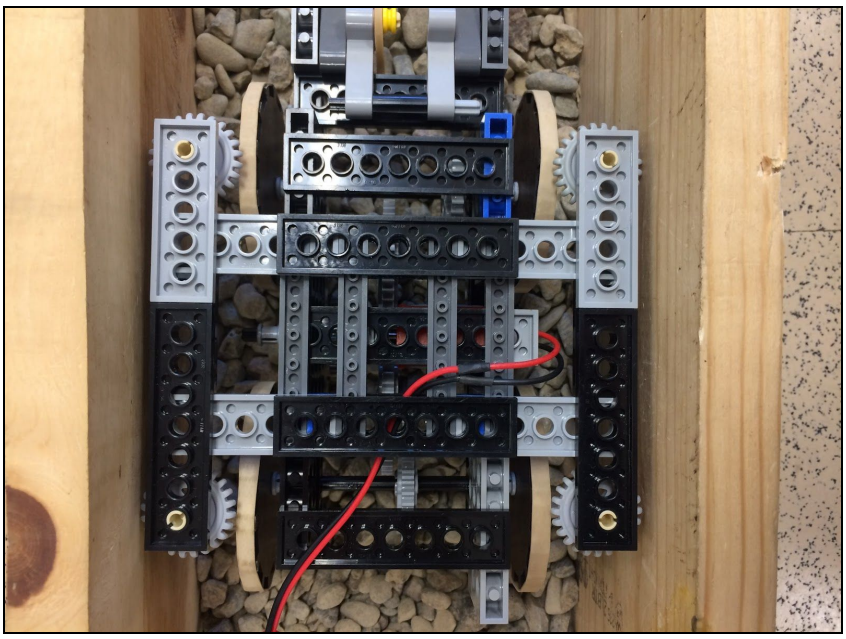

Figure 3.4.1: Linear guides and lego scaffolding

3.5 Wheel Design

Ultimately, two major considerations drove our wheel design: surmounting the steps along the track and limiting the vertical motion of the crawler in order to increase the reliability of our salamander retrieval mechanism. We also chose to mount rubber bands around the outside of the wheels in order to increase the coefficient of friction, μ. As illustrated in the free body diagram in Figure 3.5.1, a higher coefficient of friction will increase the limit of the traction force on the wheel, F_t, giving the crawler a better chance of mounting the step. Additionally, in order to minimize vertical motion and assist with mounting the steps, we iteratively created wheels that were a hybrid between smooth wheels and whegs. As illustrated in the free body diagram in Figure 3.5.2, wheels with pegs will reduce the reaction forces acting in the x-direction against the crawler's direction of travel, resulting in less power loss and more power transferred into forward motion.

After many iterations of wheel design (Figure A6.1), we selected a pegged wheel with an inner diameter of 2.5" , an outer diameter of 2.8", and 0.15' tall square pegs evenly spaced around the perimeter (Fig. 3.5.3). We laser cut the wheels from ¼' duron and stretched rubber bands around the wheels. The hard duron served to reduce rolling resistance, while the rubber bands increased the coefficient of friction. The large diameter of wheel helped our crawler mount the steps by reducing the angle of impact, θ in Fig. 3.5.1 and Fig. 3.5.2, and increased our crawler speed without altering our internal transmission or using a higher motor voltage.

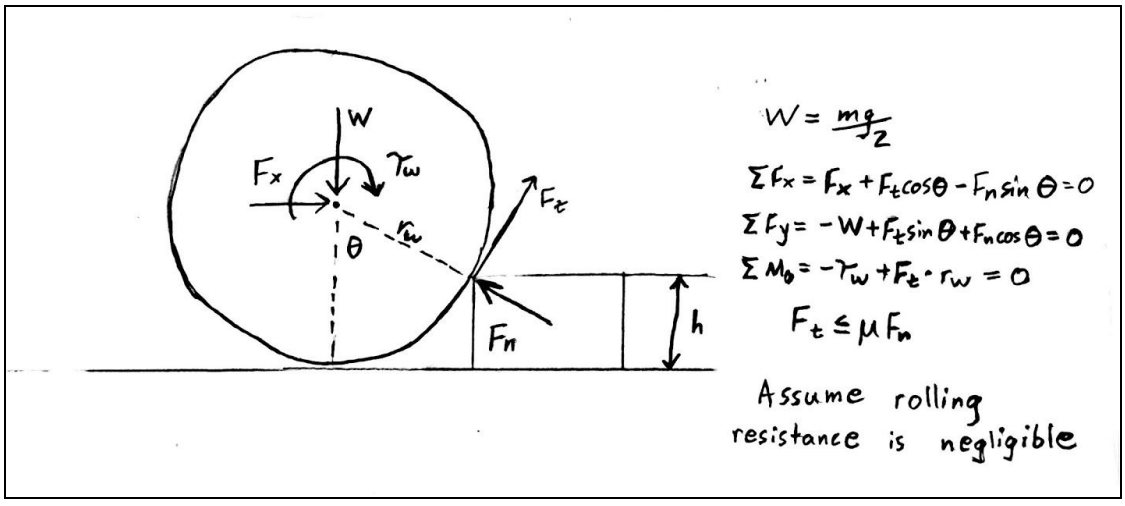

Figure 3.5.1: Free body diagram of a smooth wheel in contact with a step in the track immediately after leaving the ground

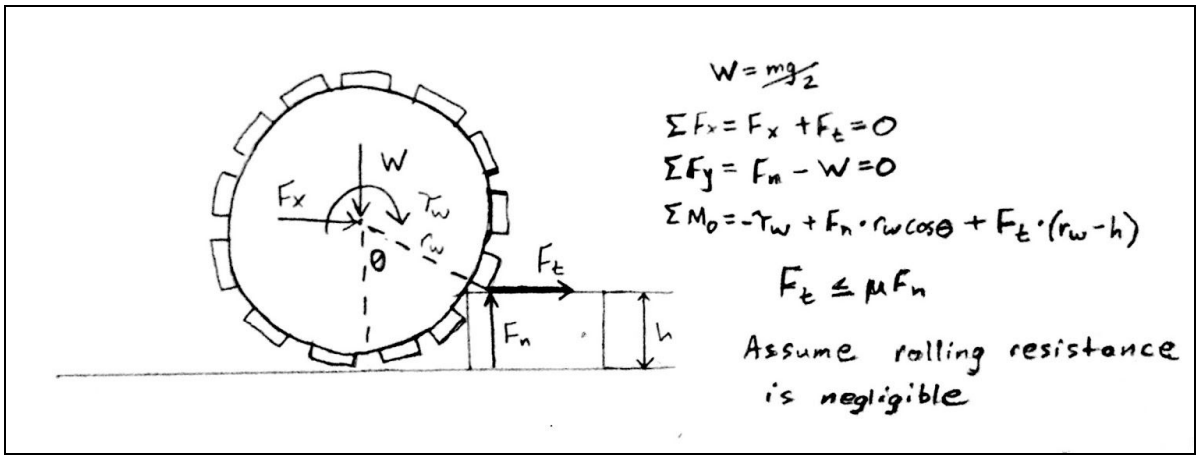

Figure 3.5.2: Free body diagram of toothed wheel mounting a step in the track immediately after leaving the ground.

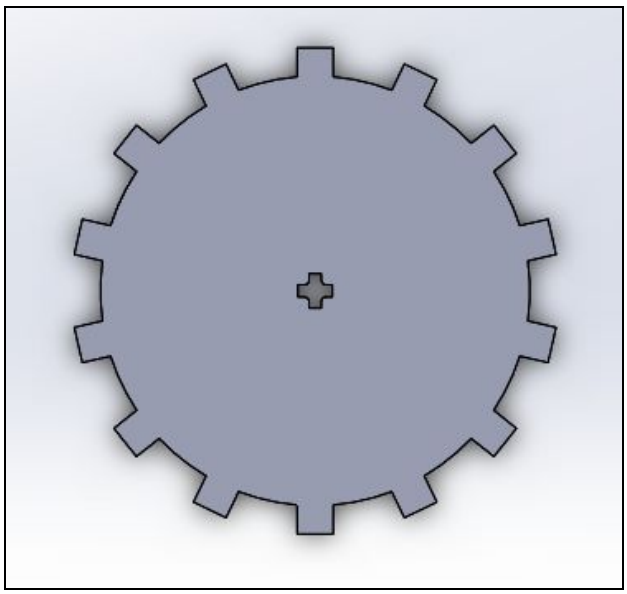

Fig. 3.5.3: *Our final wheel design (SolidWorks 2016)*

4 Logistics

The task, as described, involved traversing an uphill track, successfully clearing four half-inch steps and one and a half meters of gravel, retrieving a salamander at the end of the track, and repeating the feat in reverse whilst carrying the salamander. The salamander retrieval required successfully snatching the salamander and ensuring that the salamander remained contained throughout the reverse journey. Our design principles, simplicity, repeatability, and reliability were the keys to successfully completing this feat. We designed the salamander retrieval mechanism to be simple enough to work every time, relying on basic mechanical principles for the snatch. Simultaneously, the mechanism ensured that the salamander was securely contained during the jarring return journey, due to the tension in the rubber band and the curved wire prongs on the lever arm of the mechanism. Increasing wheel traction with rubber bands and small pegs enabled our crawler to surmount the steps in the track and maintain traction in the gravel. To reduce efficiency losses due to friction , we applied olive oil to the gear reductions in our transmission.

5 Performance Analysis

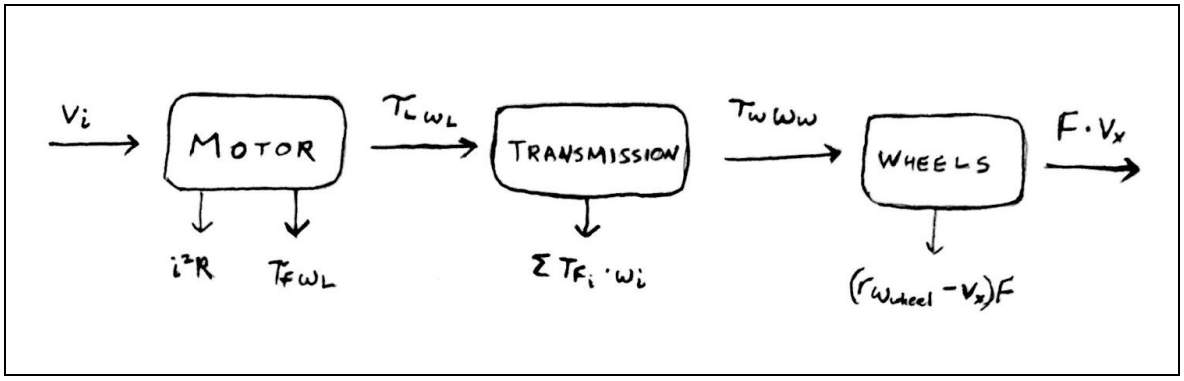

Figure 5.1.1: Schematic of power flow through our crawler system. At each stage, power is lost, reducing the overall efficiency of our crawler. We have attempted to measure and calculate each of these loss terms in order to characterize the overall efficiency of our crawler.

In our crawler system, there are three main stages at which power is lost: the motor, the transmission, and the wheels. The motor converts electrical power into mechanical rotation of the shaft; the transmission reduces the speed of mechanical rotation by 75:1 between the input and output shafts; and the wheels convert rotation and torque of the output shaft into forward motion along the track. There are inefficiencies that translate into power loss at each of these three stages. In the following sections, we measure and calculate these efficiency losses in order to characterize performance at each of these stages.

5.1 Motor Performance

The majority of the inefficiencies in our crawler originate in the crawler motor. Subsequently, we find it helpful to briefly characterize the motor. The direct-current, brushless motor operates with some amount of internal resistance, as coils of wire in the motor create a magnetic field and an additional back electromotive force (back EMF) is created. Motor characteristics and performance are defined by the voltage at which it is operating, the current that it draws, and internal characteristics k_v, the back EMF constant, and R_{motor}, an internal resistance value. Our motor equations give us:

$$V - i * R_{motor} - k_v * \omega = 0 \quad (5.2)$$

Knowing that, at stall, the angular speed (omega) of our motor is zero, we can use the current drawn by the motor (i_{stall}) to calculate the internal resistance of the motor.

$$V - i_{stall} * R_{motor} = 0 \tag{5.3}$$

To calculate this internal resistance, we found values for the current drawn by the motor at stall using varying voltages shown in Appendix 3 and found this resistance to be approximately 8.43 Ohms. Similarly, given Equation 5.2, we can use the calculated R_{motor}, the current drawn by the motor when allowed to spin freely (i_{nl}), and experimental values for our angular speed (ω) to calculate our back EMF constant k_v, approximately 0.00853. Using these values and deriving equations for the output power (A2.6), output torque (A2.4), and overall motor efficiency (A2.7), we generated the curves shown in Figures 5.1.2 and 5.1.3 to describe our motor and its performance.

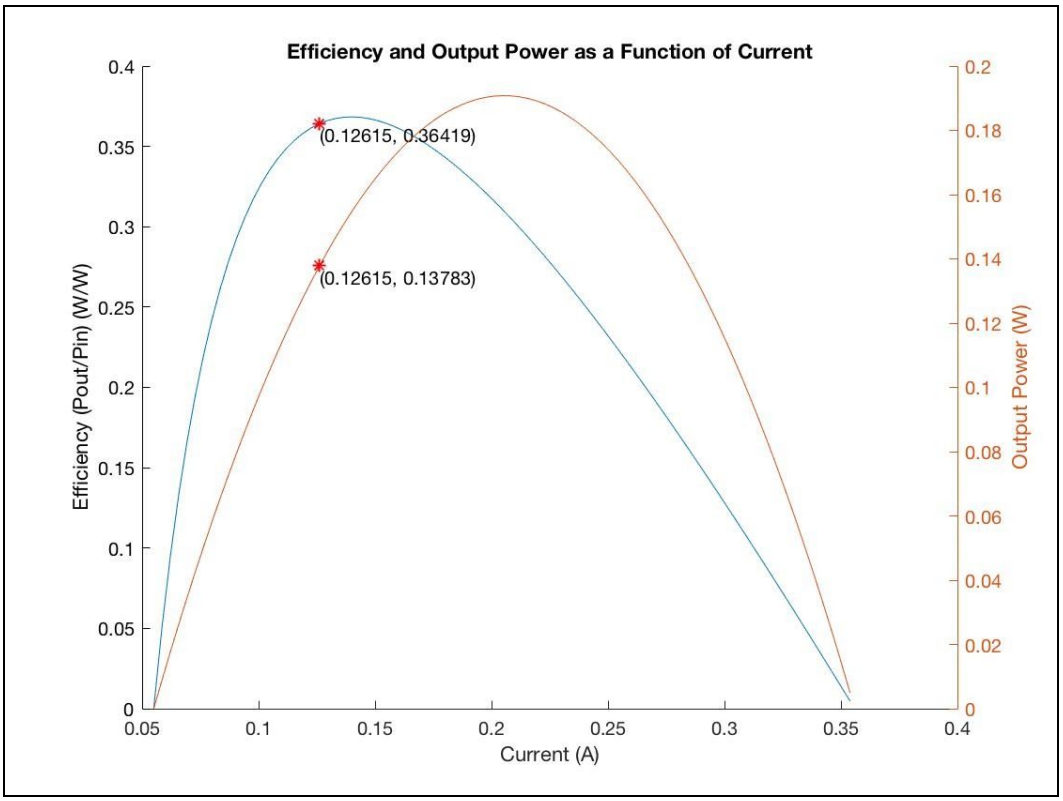

Figure 5.1.2: Motor Efficiency and Output Power varying by the motor-drawn current. The point indicated on each curve shows our final performance on test day.

During initial testing with our final crawler design, our motor was consistently drawing approximately 0.18 - 0.22 Amps. While this current value corresponds to higher output power, it denoted less efficient motor performance and as such, greater power consumption over time,

which we measure in Joules. As shown above, drawn current is a measure of the load on our motor; to reduce this load and thereby decrease our current value, we applied one drop of olive on each tooth of the smaller gears in each gear reduction pair, removing excess with absorbent cloth. In doing this, we saw a 35% reduction in the load on our motor and a 5% overall increase in our motor efficiency.

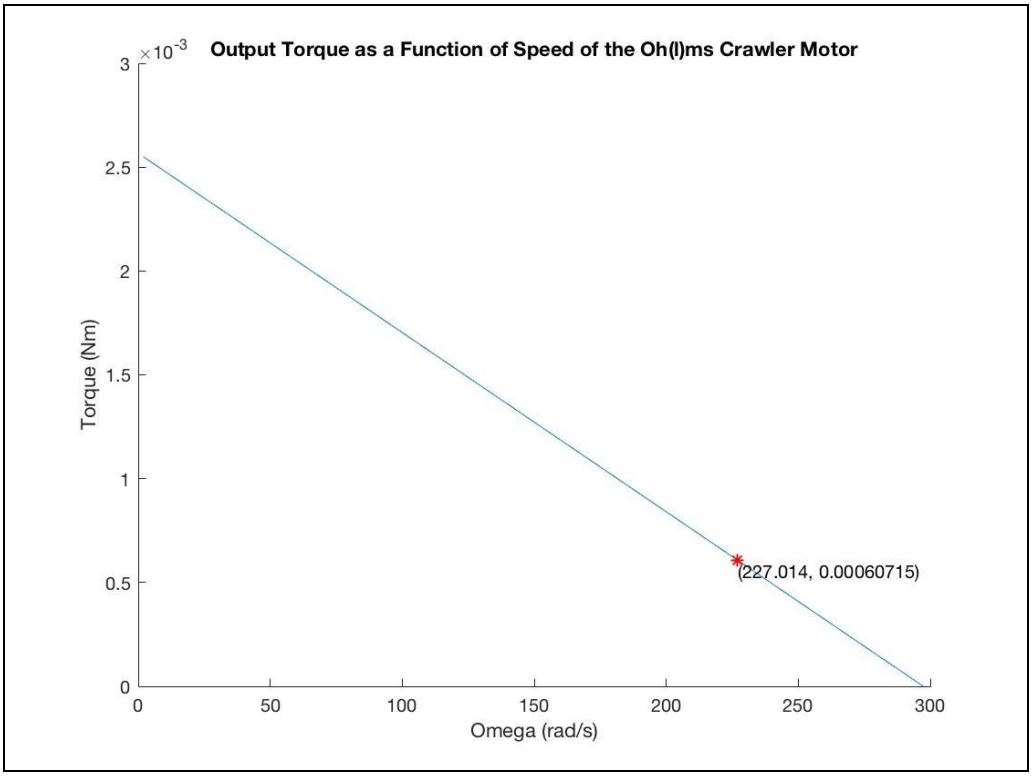

Figure 5.1.3: Output Torque of the Ohms Crawler Motor - Our crawler motor applied approximately 0.607 mNm to its axle. We utilized a gear ratio of 75:1 to increase the torque applied to our output shafts to an ideal torque of 45.4 mNm (and an actual torque of approximately 23.6 mNm accounting for the efficiency of our transmission).

Appendix 4 references a plot of motor efficiency at 3V, 6V, and 8V (Figure A4.4). Despite a higher potential motor efficiency at 6V and 8V, we chose to operate the motor at 3V. At 3V, the speed of our crawler was sufficient to both trigger the mechanical mechanism and travel through the gravel without shaking loose the salamander. We were not convinced that the speed of our crawler would increase proportionately with voltage; at a higher voltage we would expect more energy lost in collisions between the wheels and the gravel, in addition to drawing more current from our motor, using more energy and decreasing our overall efficiency. We were able to draw

current values close to peak-motor-efficiency using 3V and utilized 3.95 Joules, for a successful two test runs.

5.2 Transmission Performance

The power loss associated with our transmission system is the sum of all the frictional torques applied to each stage of our transmission, $\sum \tau_{fi} \omega_i$, which is equal to the input power of our transmission times some reduction in efficiency, η.

$$P_{loss} = \sum \tau_{fi} \omega_i = P_{in} * \eta \tag{5.4}$$

In the ideal case, with a transmission efficiency of 100%, these frictional forces would be zero, the efficiency reduction would be 1, and the ratio of torque between the input and output shafts would equal our gear reduction ratio of 75:1. However, because of the frictional forces associated with lego spline rotation and gear meshings, we know that $\eta < 1$. Therefore the relationship between our input and output torques will be:

$$\tau_{out} = \frac{\omega_{in}}{\omega_{out}} * \tau_{in} * \eta \tag{5.5}$$

Where τ_{out} is the output torque, τ_{in} is the input torque, and $\frac{\omega_{in}}{\omega_{out}}$ is the ratio of the angular velocity of our input shaft compared to the angular velocity of our output shaft (i.e. our gear ratio).

To quantify η, we isolated the transmission system and connected a drum pulley to both the input and output shafts (Figure 5.2). To more accurately model the dynamics of our actual transmission, we used a cantilevered input shaft to mimic the cantilevered input of our motor. We then hung weights from both the input and output shaft drum pulleys. This allowed us to find weights that created static equilibrium in the system: the point where the weights remained motionless and balanced but would continue to move at a constant speed after a small push.

Our transmission design employed all-wheel drive, so we conducted the pulley test on both the front and and back output axles of our transmission. For the front axle, the equilibrium weight ratio was 332g/8g, or 41.5:1. For the rear axle, the equilibrium ratio was 327g/9g, or 36.3:1. Therefore, the average of these two ratios was 38.9:1, yielding a transmission efficiency of 51.8% (38.9/75).

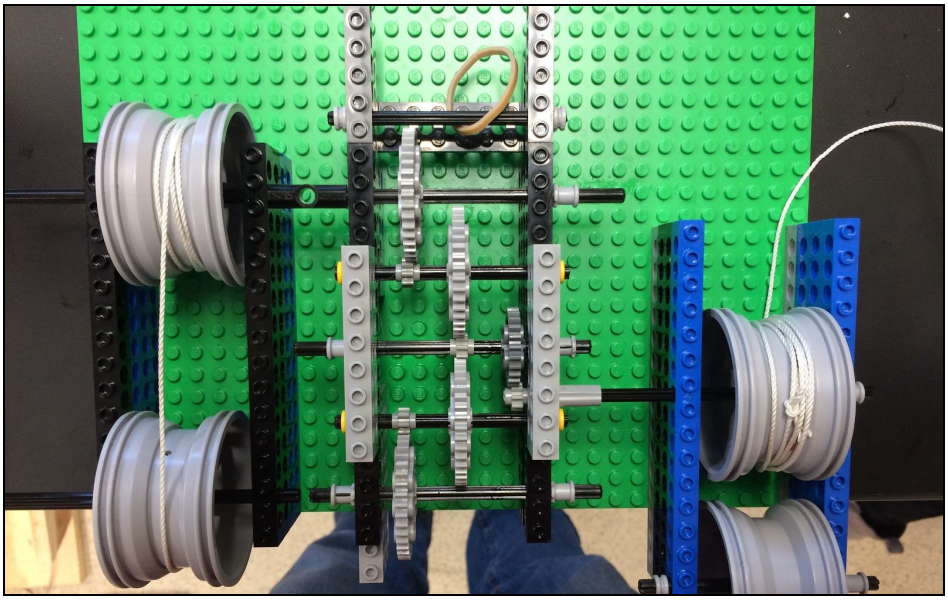

Figure 5.2: Isolated transmission system with input and output shafts connected to drum pulleys.

5.3 Rolling Resistance & Slippage

When traveling through the test tunnel, the crawler moves at a constant velocity. Therefore, all the power going to the wheels is used up to overcome rolling resistance of the track (in addition to a bit of loss due to slippage of the wheels on the ground). In a pull test of the crawler wheels connected to the transmission (but disconnected from the motor), it took approximately 42 grams of mass connected to the crawler, over a pulley, to overcome rolling resistance in the gravel section of the track (where our energy calculations are performed). Therefore, the output force of the crawler to overcome rolling resistance can be found with equation A4.1, which is 0.41202 Newtons.

Next, we investigated the effect of slippage by comparing the speed of the crawler over a given distance to the angular velocity of one of the wheels. With a high speed, Android-powered video camera, we measured an angular velocity of 4.2 radians/sec and a translational velocity of 0.134 meters/sec. This discrepancy between wheel angular velocity and horizontal speed of the whole crawler unit can be multiplied by the force found in the pull test A4.2. Hence, our crawler lost about 0.000912 Watts due to slippage of the wheels.

5.4 Efficiency Analysis

We can evaluate the overall efficiency estimate of our crawler in two ways, one of which utilizes the following equation:

$$\eta = \frac{P_{out}}{P_{in}} = \frac{F * v_x}{V * i} \tag{5.6}$$

where η, the efficiency of our crawler, is equal to the ratio between power out (force times translational velocity, $F * v_x$) and power in (voltage times current, $V * i$). The second involves calculating the efficiency at each stage and multiplying the stages together. In Figure 5.1.1, we describe the overall power flow and loss in the crawler, indicating and describing the characteristics of losses at each stage. Our model assumes that the crawler is doing a nontrivial amount of work, $F \cdot v_x$. As such, we find that rolling resistance is sufficient to calculate the efficiency of our wheels.

Our initial calculation, using the F and v_x used during our test for rolling resistance yields an overall efficiency of 18.8%. In theory, we should be able to use our test speed to calculate overall efficiency, as rolling resistance should not be speed-dependent. We examine the data for our motor and transmission efficiencies to determine whether this model is valid.

Our motor efficiency plots informed our calculations of motor efficiency, described in equation A3.7. We find that our motor was operating at an efficiency of approximately 36% (Figure 5.1.2). With our transmission operating at an average efficiency of 51.8%, we calculate the overall system efficiency before losses from the wheels at 18.6%. The theoretical efficiency discussed above is higher than our actual efficiency after two stages. We can attribute this in part to inaccuracies during testing, in particular due to over-constrained axles during the transmission tests. Additionally, the speed of the crawler did affect the amount of rolling resistance experienced, which, in this case, is more accurately described as a measure of the energy lost during collisions with the gravel on the track.

Re-calculating our overall efficiency using the v_x found during our slip test yields a value of 14.6%, which seems more reasonable, with the majority of our power loss occuring in the motor, and rolling and slip accounting for approximately 4% of our loss. The v_x value found during our slip test was not sufficiently close to our performance velocity, which varied between 0.212 and 0.172 m/s, due to insufficiently accurate test conditions, as we started the crawler on the gravel and not the smooth part of the track during the test.

5.5 Gear Strength

Interestingly, the gear that repeatedly failed in our transmission was not the gear with the most bending or contact stresses on the teeth. The second gear in our transmission, a 24-tooth, standard, dark gray Lego spur gear depicted in Figure 5.5.1 below, failed due to the long slot creating a high stress concentration close to the teeth, where forces are applied.

Fig. 5.5.1: The most failure-prone gear in our transmission

The second most failure-prone gears in our transmission are the two 8-tooth spur gears, that couple to the 40-tooth gears connected to our wheel axles. These experience the highest bending loads because the tangential forces acting on the teeth are the greatest, and they also have the smallest Lewis Form Factor. Since the motor applies an input torque of approximately 0.607 mNm, which is increased 75-fold, the torque on the output shafts should, without losses, be 45.4 mNm. The 8-tooth spur gear has an approximate pitch diameter of 9 mm, or 0.354 inches, meaning that the tangential force acting on its teeth will be the output torque divided by the pitch radius. This results in an approximate tangential force of 0.256 Newtons, or 0.058 pound-force. Other useful dimensions are summarized in the table below, and bending stress is calculated using equation A5.1.

# of gear teeth	Pitch diam. (in.)	Pitch (teeth/in. diam)	F_t (lbf)	V_t (ft/min)	Kv (AGMA)	Km (Mounting correction factor)	Ko (overload correction factor)	Lewis geometry factor, J	Allowable lifetime stress (psi)	Bending stress on teeth (psi)
8	0.354	25.4	0.058	3.717	1.0091	1.6	2	0.22	3500	173

Even when compared to a conservative allowable stress of 3500 psi for Lego plastic, the calculated bending stress on the 8-tooth spur gear is 173 psi, which yields a safety factor of roughly 20. Therefore, given the current design of our transmission, all gears, with the exception of the 24-tooth slotted one, should comfortably resist failure. In future iterations, we would like to replace the constantly-failing 24-tooth gear with a more geometrically stable gear.

6 Conclusion and ReDesign

Our crawler performed exactly as designed, with current drawn at 3V nearly equal to the peak efficiency projected in our analysis. The salamander catching mechanism works with incredible reliability - in the final iteration, the mechanism has never failed to pick up and secure the salamander in any test run or competition run. The crawler travels more or less straight along the tunnel, thanks to the linear guides. The transmission ratio gives a manageable and safe speed of travel, while not being painstakingly slow. The wheels work well on both the gravel and wood of the test tunnel. The one major hiccup with our design is the use of the gray 24-tooth gear in the first stage of the transmission. Three of these gears have cracked over the span of a few weeks of testing. It would be ideal to replace this with a more robust 24-tooth gear.

Were this challenge to be repeated with a 250g salamander, our crawler would require significant alterations. Starting from the front of the crawler, our catching mechanism would likely need to use a stronger rubber band in order to lift the heavier salamander. Additionally the “forks,” which pick up the salamander, might require reinforcement. Our crawler weighed approximately 206 grams, with a center of mass close to the middle of the crawler. Hence, a 250 gram salamander at the front would likely tip the crawler forward, in addition to making it more difficult to get over the half-inch steps along the tunnel. This can be addressed with two solutions. The first would be to increase the weight of the rear of the crawler with ballast. The second would be to move the front axle forward, so as to reduce the effective torque of the salamander about the pivot of the point of front wheel contact.

In addition to these changes to the mechanism and body, it would likely be necessary to move to a higher gear reduction, in order to provide sufficient torque to lift the crawler up and over the four half-inch steps. In our testing, this was the point at which the crawler needed the most torque. An increased gear reduction would make the crawler slower and possibly less efficient depending on the need to increase the number of stages and change gear sizes.

7 Appendices

A1 - Symbols and Definitions

Symbol	Definition	Units
V	Voltage from power source	Volts
i	Current from power source	Amps
R_{motor}	Internal resistance of the motor	Ohms
F_{roll}	Force to overcome rolling resistance	Newtons
m_{cup}	Mass in cup on end of pulley to pull crawler in rolling test	grams
g	Acceleration due to gravity	meters/s^2
P_{slip}	Power lost due to wheel slippage on ground	Watts
ω_{wheel}	Angular velocity of wheel during test	radians/sec
r_{wheel}	Radius of the wheels	meters
v_x	Horizontal speed of crawler during test	meters/second
σ_b	Bending stress on gear teeth	lb/in^2
F_t	Tangential force on gear teeth	Newtons
P	Gear pitch	teeth/inch diam.
b	Gear face width	inches
J	Lewis geometry factor	unitless
K_m	Mounting correction factor	unitless
K_o	Overload correction factor	unitless
K_v	Velocity correction factor	unitless
k_v	Back-EMF Constant	radians/(Volts*sec)
i_{stall}	Current at stall	Amps
ω	Angular speed	radians/second
i_{nl}	Free-spinning current	Amps
η	Efficiency	unitless

τ	Torque	Newton*meter
P	Power	Watts

A2 - Motor Equations and Derivations

$$V - i * R_{motor} - k_v * \omega = 0 \quad 5.2$$

$$V - i_{stall} * R_{motor} = 0 \quad 5.3$$

$$V - i_{nl} * R_{motor} - k_v * \omega_{nl} = 0 \quad A2.1$$

$$T_L = T_m - T_f \quad A2.2$$

$$T_m = k_v * i \quad A2.3$$

$$T_f = k_v * i_{nl} \quad A2.4$$

$$P_{out} = T_L * \omega \quad A2.5$$

$$P_{out} = \frac{(k_v * i - T_f)(V - iR)}{k_v} \quad A2.6$$

$$\eta_{motor} = \frac{P_{out}}{P_{in}} = \frac{T_L \omega}{V i} = \frac{(V - iR)}{k_v} * \frac{(k_v i - T_f)}{V i} \quad A2.7$$

A3 - Motor Graphs and Data

Voltage (V)	i_{stall} (A)	R_{motor} (Ω)
1.5	0.19	7.894736842
2.5	0.31	8.064516129
3.5	0.42	8.333333333
4.5	0.52	8.653846154
5.5	0.63	8.73015873
6.5	0.73	8.904109589
7.5	0.83	9.036144578

Figure A3.1: Calculated R_{motor} values. We deemed the last test value an outlier due to the potential of overheating the motor, which affects the resistance value but is not a part of our model. We thus omitted the value from further calculations.

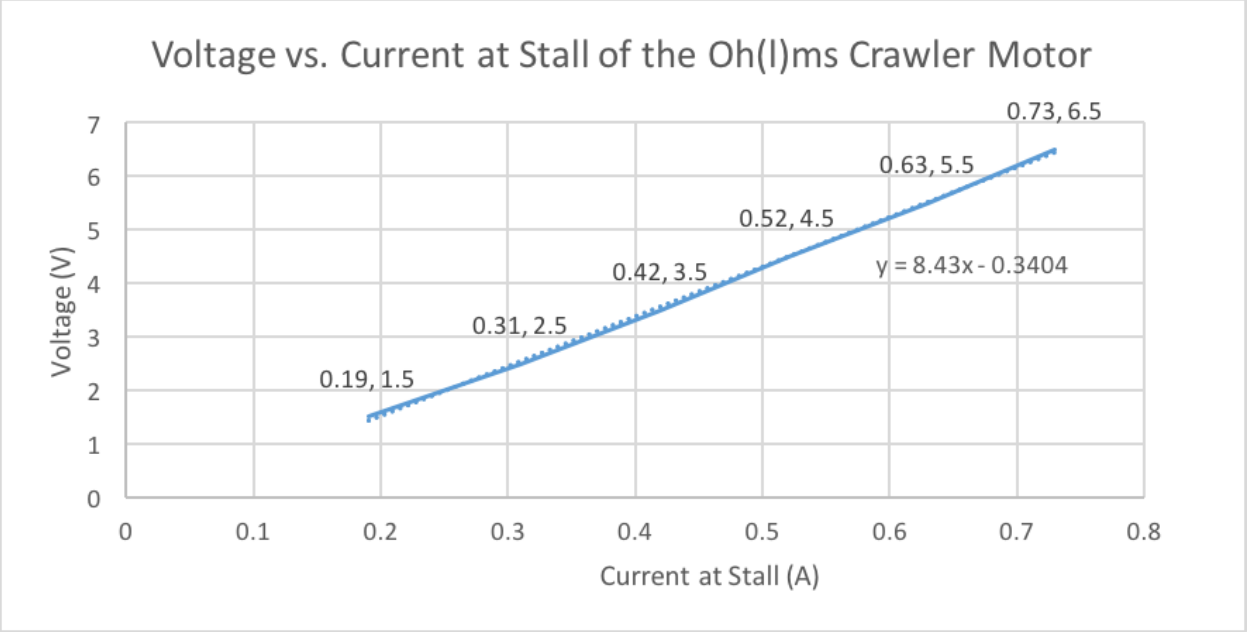

Figure A3.2: Calculated Resistance Values for the Oh(l)ms Crawler motor. The displayed trendline indicates the average calculated R_{motor} - the slope of the trendline.

Voltage (V)	i_{nl}	rpm	ω_{nl}	$V-i_{nl}*R_{motor}$	k_v
1.5	0.04	2600	136.1356817	1.162795328	0.008541444
2.5	0.05	4730	247.6622209	2.07849416	0.008392455
3.5	0.06	6700	350.8111797	2.994192992	0.008535056
4.5	0.07	8630	451.8657433	3.909891824	0.008652773

Figure A3.3: Table of values used to calculate k_v for the Oh(l)ms Crawler motor

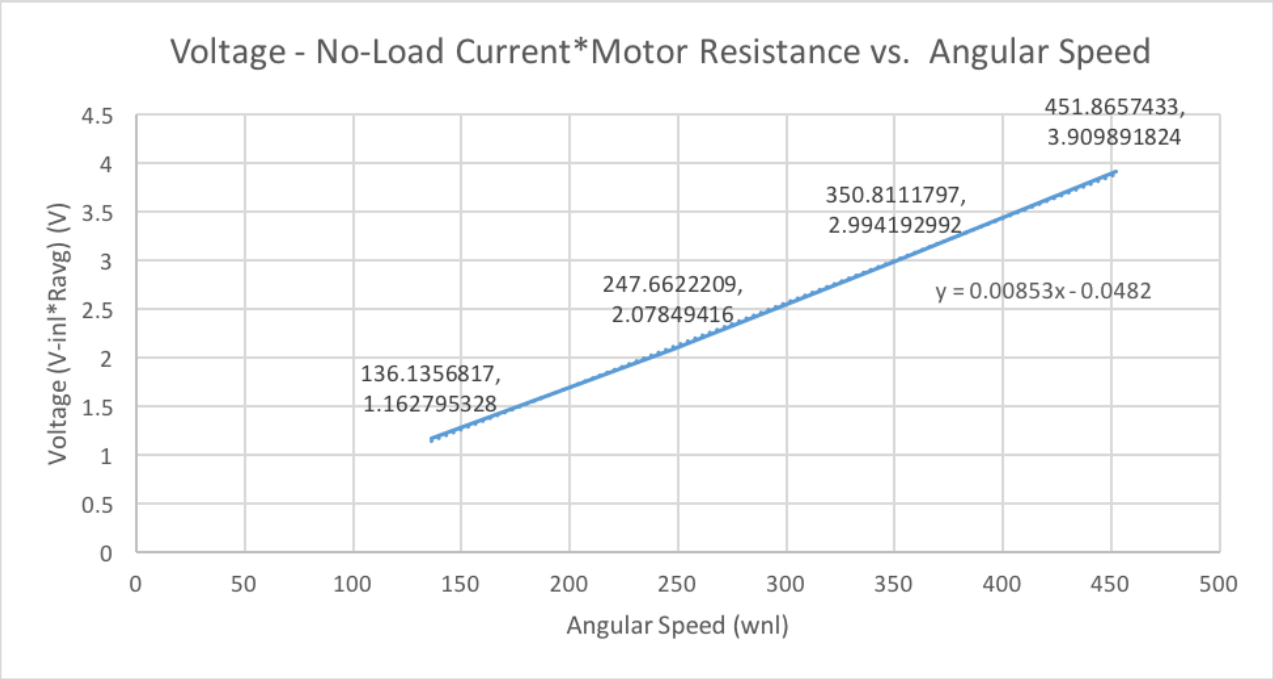

Figure A3.4: Calculated back EMF constant values for the Oh(l)ms Crawler motor. The displayed trendline indicates the average calculated k_v - the slope of the trendline.

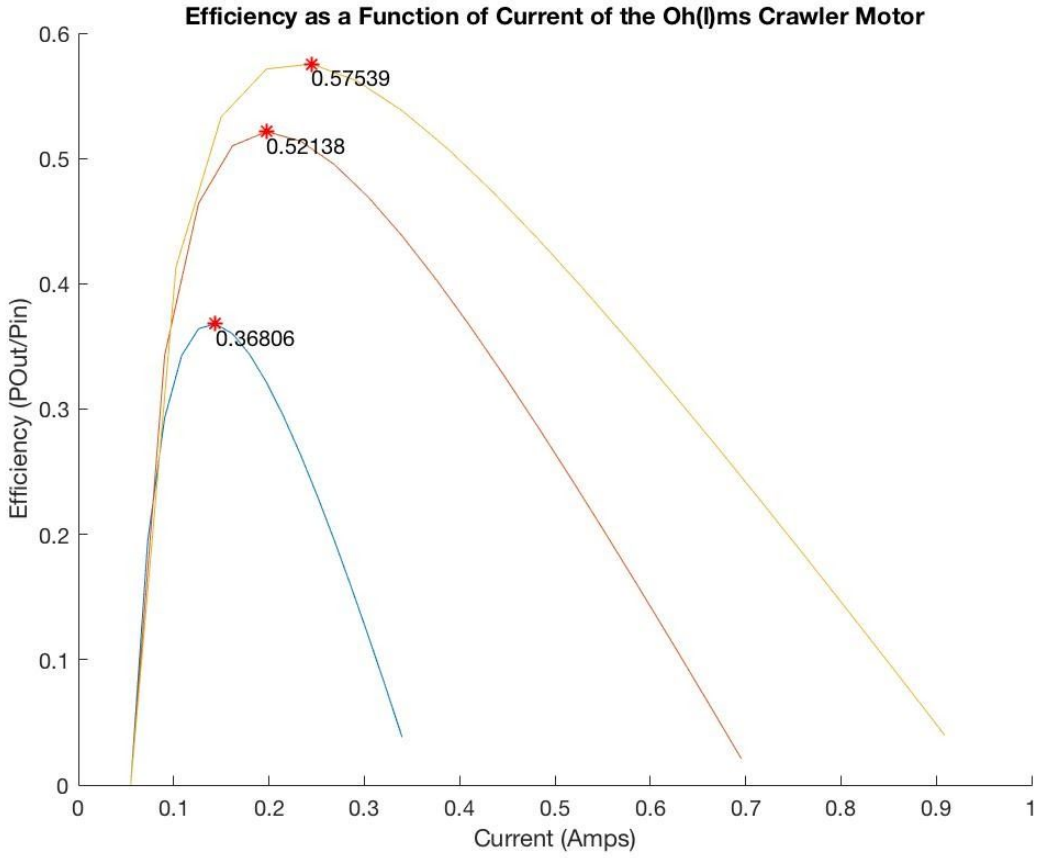

Figure A3.5: Peak Efficiency Values for the Oh(l)ms Crawler Motor as a Function of Current for all three voltages (3V, 6V, and 8V)

i (A)	ω (rad/s)	T_l (Nm)	P_{in} (W)	P_{out} (W)	η_{motor}
0.054979837	297.3506489	0	0.16493951	0	0
0.072773431	279.7664794	0.000151786	0.218320293	0.042464768	0.194506739
0.090567025	262.1823098	0.000303573	0.271701076	0.079591458	0.292937589
0.10836062	244.5981403	0.000455359	0.325081859	0.11138007	0.34262161
0.126154214	227.0139707	0.000607146	0.378462642	0.137830603	0.364185491
0.143947808	209.4298011	0.000758932	0.431843425	0.158943058	0.368057146
0.161741403	191.8456316	0.000910719	0.485224208	0.174717435	0.360075677

0.179534997	174.261462	0.001062505	0.538604991	0.185153734	0.343765351
0.197328591	156.6772925	0.001214292	0.591985774	0.190251954	0.321379267
0.215122186	139.0931229	0.001366078	0.645366557	0.190012096	0.294425073
0.23291578	121.5089533	0.001517865	0.69874734	0.184434159	0.263949712
0.250709374	103.9247838	0.001669651	0.752128123	0.173518145	0.230702908
0.268502968	86.34061423	0.001821438	0.805508905	0.157264052	0.195235646
0.286296563	68.75644467	0.001973224	0.858889688	0.13567188	0.157961939
0.304090157	51.17227511	0.002125011	0.912270471	0.108741631	0.119198894
0.321883751	33.58810555	0.002276797	0.965651254	0.076473303	0.079193501
0.339677346	16.003936	0.002428584	1.019032037	0.038866897	0.038140996

Figure A3.6: Table of Motor Curve Values (current, angular velocity, output torque, input power, output power, and efficiency) at 3V, using R_{motor} = 8.43 Ohms, k_v =0.00853

A4 - Tests and Equations for Tests (Rolling, Transmission Efficiency)

$$F_{roll} = m_{cup} * g \quad \text{A4.1}$$

$$P_{slip} = F_{roll} * (\omega_{wheel} * r_{wheel} - v_x) \quad \text{A4.2}$$

A5 - Strength Calculations

$$\sigma_b = [(F_t * P) / (b * J)] * K_m * K_o * K_v \quad \text{A5.1}$$

A6 - Previous Prototypes

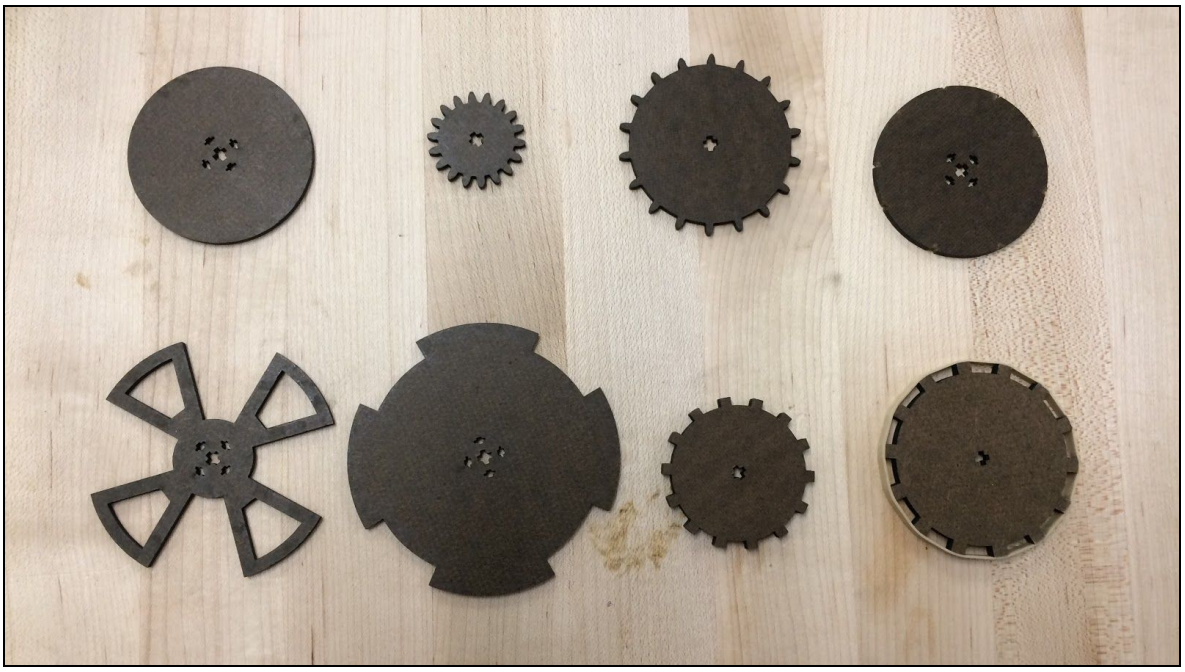

Figure A6.1: Iterative wheel design, with earliest prototype wheels in the top left and final crawler wheels with rubber bands in the bottom right.

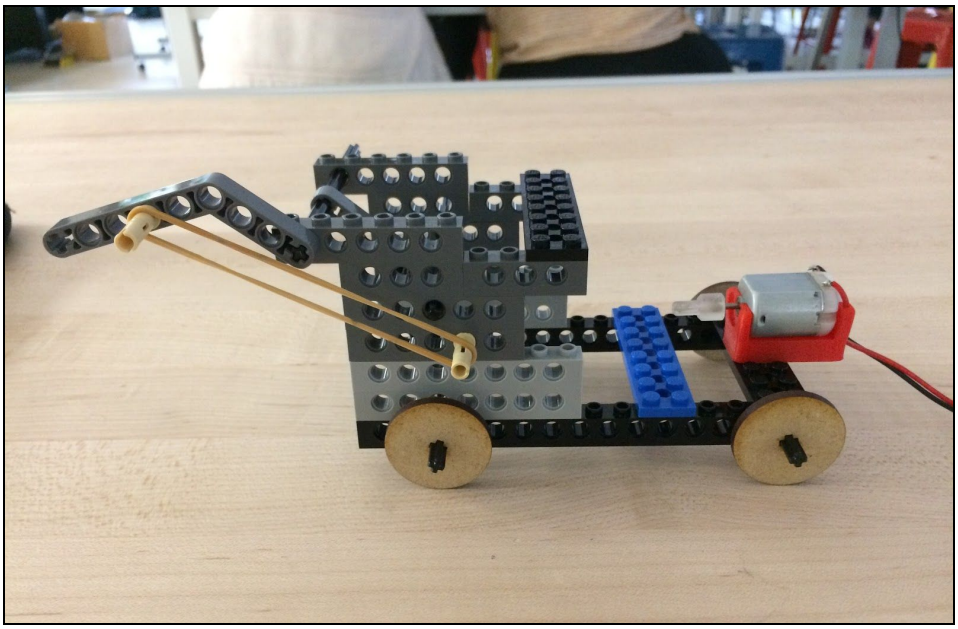

Figure A6.2: The first early prototype of the salamander retrieval mechanism, which consists only of a lever arm, an axle, and a rubber band.

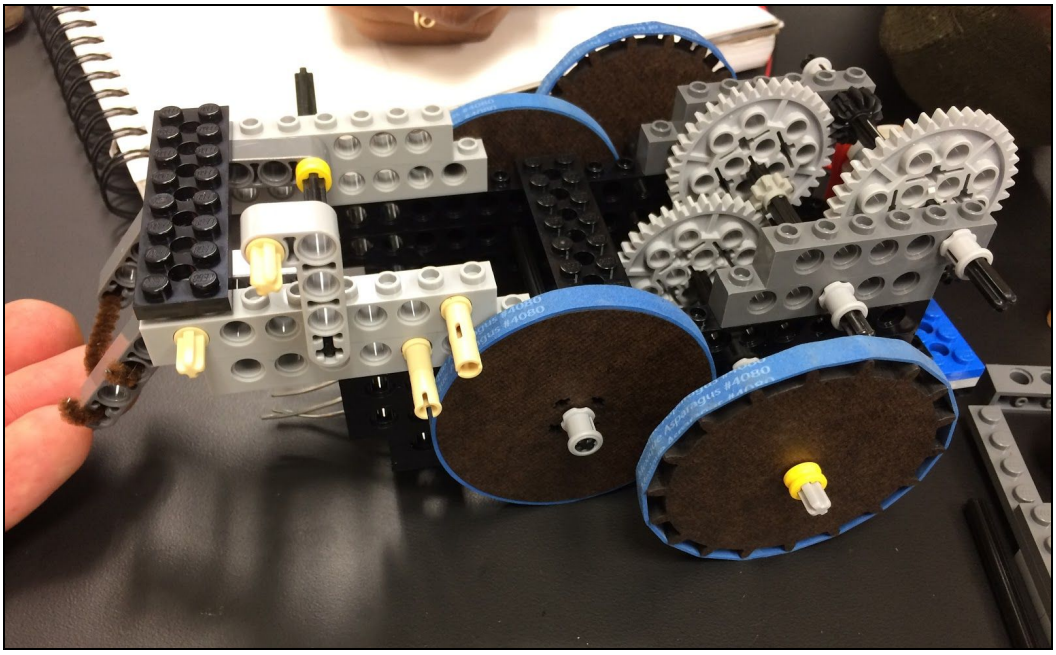

Figure A6.3: An early prototype of a full-crawler complete with transmission, wheels, and an alternative retrieval mechanism.

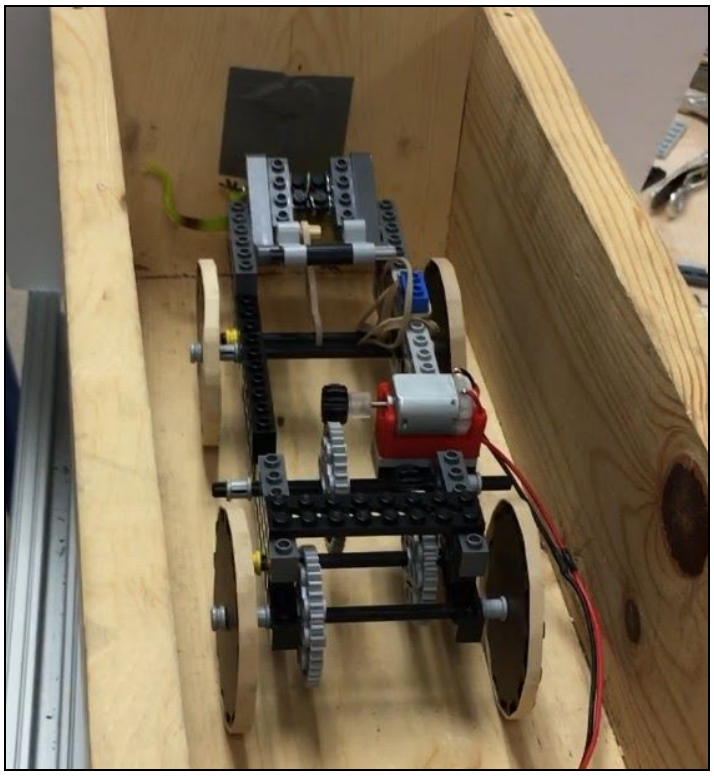

Figure A6.4: Working mechanism with rear-wheel drive transmission. This transmission was unable to return with the salamander due to the center of gravity of the vehicle.

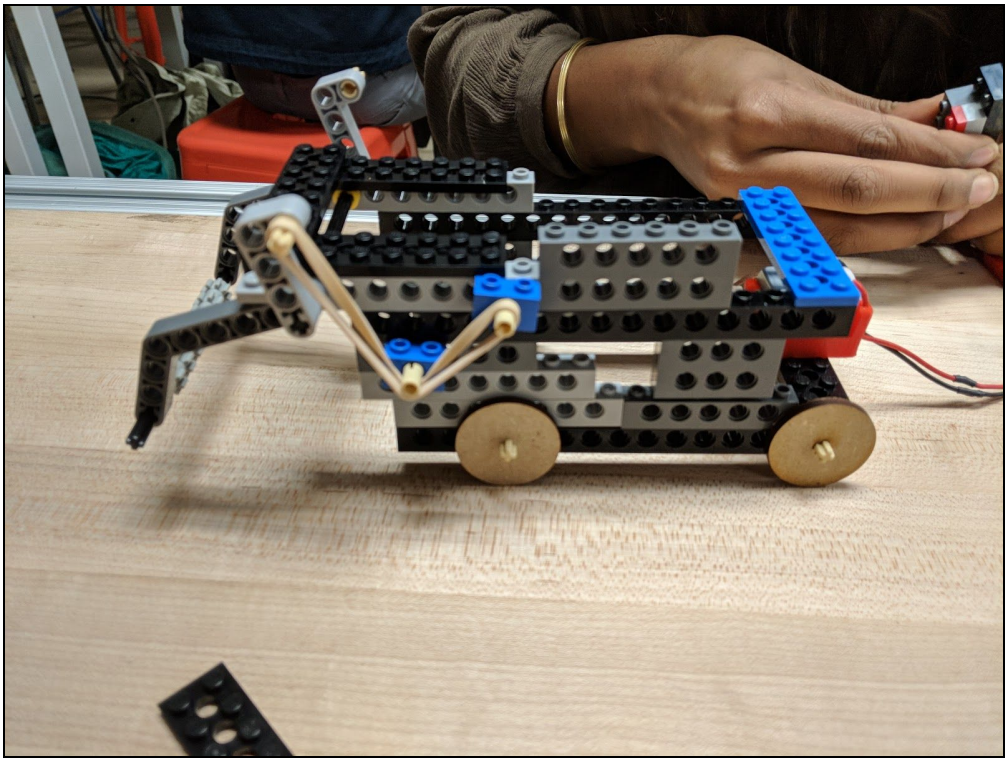

Figure A6.5: A prototype of a different mechanically triggered, rubber-band loaded salamander retrieval mechanism.